Cancellation properties in Hall magnetohydrodynamics with a strong guide magnetic field

L. N. Martin,[1] G. De Vita,[2] L. Sorriso-Valvo,[3,4] P. Dmitruk,[1] G. Nigro,[2] L. Primavera,[2] and V. Carbone[2]

[1]*Departamento de Física, Facultad de Ciencias Exactas y Naturales, Universidad de Buenos Aires and IFIBA, CONICET, Buenos Aires 1428, Argentina*

[2]*Dipartimento di Fisica, Università degli Studi della Calabria, 87036 Rende, Cosenza, Italy*

[3]*CNR, IPCF, UOS di Cosenza, 87036 Rende, Cosenza, Italy*

[4]*Space Sciences Laboratory, University of California, Berkeley, Berkeley, California 94720, USA*

(Received 28 June 2013; revised manuscript received 15 November 2013; published 18 December 2013)

We present a signed measure analysis of compressible Hall magnetohydrodynamic turbulence with an external guide field. Signed measure analysis allows us to characterize the scaling behavior of the sign-oscillating flow structures and their geometrical properties (fractal dimensions of structures). A reduced numerical model, valid when a strong guide magnetic field is present, is used here. In order to discuss the effect of the Hall term, different values for the ion skin depth are considered in the simulations. Results show that as the Hall term is increased, the fractal dimension of the current and vorticity sheets decreases. This observation, together with previous analysis of the same fields, provides a comprehensive description of the effect of the Hall force on the formation of structures. Two main processes are identified, namely, the widening and unraveling of the sheets.

DOI: 10.1103/PhysRevE.88.063107 PACS number(s): 52.30.Cv, 05.45.Df, 47.27.De, 52.25.Xz

I. INTRODUCTION

Magnetohydrodynamics (MHD) is a reasonable theoretical framework to describe the large-scale dynamics of a plasma. However, when a more detailed description is needed (for instance, when the physical context favors the development of small scales) it is most appropriate to consider two-fluid models. Two-fluid effects can be considered through a generalized Ohm's law that includes the Hall current, which is required for phenomena with characteristic length scales comparable to or smaller than the ion skin depth c/ω_{pi} (c is the speed of light and ω_{pi} is the ion plasma frequency). Among its manifestations, the Hall current causes the magnetic field to freeze in the electron flow instead of being carried along with the bulk velocity field (in an ideal plasma). Another important feature of the ideal Hall MHD description is the self-consistent presence of electric fields parallel to the mean magnetic field. Hall MHD has recently been invoked in advancing our understanding of phenomena ranging from dynamo mechanisms [1], magnetic reconnection [2–4], and accretion disks [5,6] to the physics of turbulent regimes [7–10].

In many cases of interest, such as in fusion devices or geophysical and astrophysical plasmas, a strong externally supported magnetic field is present. For such cases, an alternative reduced model was proposed, an extension of the previously known reduced MHD (RMHD) model to include the Hall effect (the RHMHD model) [11–13]. In this approximation, the fast compression Alfvén mode is eliminated, while the shear Alfvén and the slow magnetosonic modes are retained [14]. The RMHD equations have been used to investigate a variety of problems such as current sheet formation [15,16], nonstationary reconnection [17,18], the dynamics of coronal loops [19–22], and the development of turbulence [23]. The self-consistency of the RMHD approximation has been analyzed in Ref. [24]. Moreover, numerical simulations have been used to assess the validity of the RMHD equations by directly comparing its predictions with compressible MHD equations in a turbulent regime [25]. The validity of the RHMHD model has also been studied in the same way [12].

The properties of small-scale structures in magnetohydrodynamic and Hall magnetohydrodynamic turbulence have recently been studied extensively. Particular attention has been paid to the geometrical properties of current sheets in Hall magnetohydrodynamics (HMHD), as these structures are associated with magnetic flux reconnection and magnetic energy dissipation, processes of utmost importance in astrophysics and space physics [10,26–28].

However, studies have provided conflicting results so far, so the debate on the effect of the Hall term on the generation of turbulent structures is still open. For example, some recent numerical simulations have indicated that current sheets in the presence of the Hall effect become wider than in MHD (see, e.g., [29]), while other studies have shown the presence of thinner structures [30].

Previous studies of turbulent HMHD have shown that the peak of the spectrum of the current density is located at a wave number corresponding to the inverse of the ion skin depth [1,8,31,32]. Since this peak can be associated with the average thickness of the current sheets, the shift of the peak was interpreted as a thickening of the current sheets with increasing Hall effect [33]. This result is in good agreement with experimental observations, which confirm that the current sheets thickness in the presence of the Hall effect is indeed given by the ion skin depth [34].

In contrast, other studies have observed the formation of thinner structures when the Hall effect increases, suggesting that HMHD is more intermittent than MHD [30]. This was also observed in solar wind turbulence, e.g., using the Cluster spacecraft magnetic data [35,36]. Incidentally, other instances of solar wind observations of high-frequency magnetic field fluctuations from the same spacecraft indicated that while large scales are compatible with multifractal intermittent turbulence, small scales show non-Gaussian self-similarity [37].

Using the set of simulations that will be studied here, in a previous paper the effect of the Hall term was analyzed in terms of global magnitudes (e.g., the mean square current density $\langle j^2 \rangle$ and vorticity $\langle \omega^2 \rangle$), characteristic times of the flow, energy cascade, and qualitative features of the flow structures (current sheets) [29]. The Hall term turned out to affect mostly the scales between the Hall scale and the dissipation scale. This produces an enhancement of the energy transfer in such a scale range and therefore the accumulation of energy decreases. This corresponds to an effective shift of the dissipation scale toward smaller scales. This was estimated by observing an increasingly sharp steepening of the energy spectrum in the Hall range, when the separation between the Hall scale and the dissipation scale is larger. This suggests the possible generation of smaller scales when the Hall effect increases. Qualitative observation of current sheets showed that they become wider as the Hall effect increases; however, within them, smaller structures seem to emerge.

In another paper [38], a detailed and rigorous study of intermittency was performed. In the presence of the Hall effect, field fluctuations at scales smaller than the ion skin depth become substantially less intermittent, with scaling properties close to self-similarity. The quality of the numerical simulations was also tested, according to the stringent criteria of Wan *et al.* [39].

The quantitative measure of the intermittency is crucial to understand the distribution of dissipation in magnetofluids and plasmas and can also provide constraints for the theoretical study of phenomena such as magnetic energy dissipation and reconnection. Following recent results as briefly summarized above, it is thus not clear whether Hall magnetohydrodynamic small-scale structures are thinner than in MHD, making HMHD more intermittent than MHD, or, on the contrary, they are more space filling, causing intermittency to decrease because of the Hall effect. The main purpose of the present paper is to quantitatively evaluate the characteristics of the small-scale structures and their features with respect to the magnitude of the Hall effect.

In order to gain more insight into the actual effect of the Hall term on flow structures, here we study the geometrical properties of the vorticity and current field, using an explicit and quantitative approach. Our study focuses on the estimation of the cancellation exponents, as introduced by Ott *et al.* [40]. Such exponents provide a simple characterization of the flows and are phenomenologically related to the fractal dimension of the typical structure [41]. Finally, corroborated by the aforementioned studies, we show that the Hall effect affects current sheets mainly in two ways. On the one hand, the current (and vorticity) sheets widen, while on the other hand they unravel, reaching a more complex structure. This fragmentation, which could be seen as the formation of microsheets, turns out to be increasingly evident as the Hall effect increases.

The present paper is organized as follows. In Sec. II the set of equations describing the reduced Hall MHD is described. The details of the numerical simulations are given in Sec. III. In Sec. IV the main idea of the cancellation analysis technique is introduced. Finally, the results are presented in Sec. V and discussed in Sec. VI.

II. REDUCED MHD AND HMHD MODELS

For a compressible flow, the HMHD equations can be written (in dimensionless form) as

$$\frac{\partial \mathbf{u}}{\partial t} - \mathbf{u} \times \boldsymbol{\omega} = -\nabla\left(\frac{\mathbf{u}^2}{2} + \frac{\rho^{\gamma-1}}{M_S^2(\gamma-1)}\right) + \frac{1}{M_A^2}\frac{\mathbf{J}\times\mathbf{b}}{\rho} + \nu\frac{\nabla^2\mathbf{u}}{\rho} + \left(\delta + \frac{1}{3}\nu\right)\frac{\nabla(\nabla\cdot\mathbf{u})}{\rho}, \tag{1}$$

$$\frac{\partial \mathbf{A}}{\partial t} - \mathbf{u}\times\mathbf{b} = -\epsilon\frac{\mathbf{J}\times\mathbf{b}}{\rho} - \nabla\phi + \eta\nabla^2\mathbf{A}, \tag{2}$$

$$\frac{\partial \rho}{\partial t} + \nabla\cdot(\rho\mathbf{u}) = 0, \tag{3}$$

$$\nabla\cdot\mathbf{A} = 0. \tag{4}$$

In these equations, $\mathbf{u}$ is the velocity field, $\boldsymbol{\omega}$ is the vorticity field, $\mathbf{J}$ is the current, $\mathbf{b}$ is the magnetic field, ρ is the density of the plasma, and $\mathbf{A}$ and ϕ are the magnetic and electric potentials, respectively. A barotropic law is assumed for the plasma, with the pressure given by $p = C\rho^\gamma$, where C is a constant and $\gamma = 5/3$. Equation (4) is the Coulomb gauge, which acts as a constraint that fixes the electric potential in Eq. (2). The control parameters of the system are the sonic Mach number M_S, the Alfvén Mach number M_A, the viscosities ν and δ (here we consider $\nu = \delta$), and the resistivity η. In our study, the most important control parameter is the Hall coefficient $\epsilon = \rho_{ii}/L$, where ρ_{ii} is the ion skin depth and L is the characteristic scale of turbulence. When $\epsilon = 0$, the equations above result in the well known compressible MHD equations.

In the presence of a strong guide field, Eqs. (1)–(4) can be written using the reduced approximation often used in magnetohydrodynamics (see, e.g., [42,43]). The approximation assumes that the magnetic field can be written as

$$\mathbf{b} = B_0\hat{\mathbf{z}} + \mathbf{b}', \tag{5}$$

where B_0 is the intensity of the guide magnetic field aligned with the $\hat{\mathbf{z}}$ direction and $\mathbf{b}'$ is such that $|\mathbf{b}'|/B_0 \ll 1$.

For convenience, when writing the dimensionless equations we assume, without loss of generality, that $B_0 = 1$. We then decompose the velocity and magnetic field fluctuations in terms of scalar potentials as

$$\mathbf{u} = \nabla\times(\varphi\hat{\mathbf{z}} + f\hat{\mathbf{x}}) + \nabla\psi \tag{6}$$

and

$$\mathbf{b}' = \nabla\times(a\hat{\mathbf{z}} + g\hat{\mathbf{x}}). \tag{7}$$

Equation (7) ensures that the magnetic fields remain divergence-free, while Eq. (6) gives us a compressible flow. The potentials f and g allow for dynamical components of the fields parallel to the guide field and ψ describes an irrotational component of the velocity field.

Then Eqs. (1)–(4) can be written as (for the details see [11–13,29])

$$\frac{\partial u}{\partial t} = \frac{\partial b}{\partial z} + [\varphi,u] - [a,b] + \nu\nabla^2 u, \tag{8}$$

$$\frac{\partial \omega}{\partial t} = \frac{\partial j}{\partial z} + [j,a] - [\omega,\varphi] + \nu\nabla^2\omega, \tag{9}$$

$$\frac{\partial a}{\partial t} = \frac{\partial(\varphi - \epsilon b)}{\partial z} + [\varphi, a] - \epsilon[b, a] + \eta\nabla^2 a, \tag{10}$$

$$\frac{\partial b}{\partial t} = \beta_p \frac{\partial(u - \epsilon j)}{\partial z} + [\varphi, b] + \beta_p[u, a] - \epsilon\beta_p[j, a] + \eta\beta_p\nabla^2 b, \tag{11}$$

where

$$u = -\partial_y f, \tag{12}$$

$$\omega = -\nabla_\perp^2 \varphi, \tag{13}$$

$$b = -\partial_y g, \tag{14}$$

$$j = -\nabla_\perp^2 a, \tag{15}$$

and the notation $[A, B] = \partial_x A \partial_y B - \partial_x B \partial_y A$ is employed for the Poisson bracket. The potential ψ was eliminated from these equations using the equation for the pressure. Finally, $\beta_p = \beta\gamma/(1 + \beta\gamma)$ is a function of the plasma beta. As in the previous set of equations, these equations become the compressible RMHD equations when $\epsilon = 0$.

III. NUMERICAL SIMULATIONS

The simulations analyzed in this work are similar to those described in Ref. [29]. We use a standard parallel pseudospectral code to evaluate the nonlinear terms and solve the equations numerically [44]. A second-order Runge-Kutta time integration scheme is used. The magnetic field fluctuations in all simulations are less than 10% of the external magnetic field value, so we are in the range of validity of the RHMHD model. Periodic boundary conditions are assumed in all directions of a cube of side $2\pi L$ (where $L \sim 1$ is the initial correlation length of the fluctuations, defined as the length unit). The runs performed throughout this paper do not contain any magnetic or velocity external stirring terms, so the RHMHD system is let to evolve freely. To generate the initial conditions, we excite initially Fourier modes (for both magnetic and velocity field fluctuations) in a shell in k space with wave numbers $1 \leqslant k \leqslant 2$, with the same amplitude for all modes and with random phases. Only plane-polarized fluctuations (transverse to the mean magnetic field) are excited, so the initial conditions are Alfvén mode fluctuations with no magnetosonic modes. In the set of simulations, the spatial resolution is 512^2 grid points in the plane perpendicular to the external magnetic field and 32 grid points in the parallel direction. In fact, higher resolution is required in the planes perpendicular to B_0, with respect to the parallel direction. This is due to the fact that the dynamics of the system generates structures mostly along the direction perpendicular to B_0. The kinetic and magnetic Reynolds numbers are defined as $R = 1/\nu$ and $R_m = 1/\eta$, respectively, based on unit initial rms velocity fluctuation, unit length, and dimensionless values for the viscosity and diffusivity. For all the runs, we used $R = R_m = 1600$ (i.e., $\nu = 1/1600$ and $\eta = 1/1600$). We also considered a Mach number $M_S = 1/4$ and an Alfvén Mach number $M_A = 1$.

Four values of the Hall parameter are considered, namely, $\varepsilon = 0$ (the MHD case), 1/32, 1/16, and 1/8. Data from simulations with such values of ε are labeled as runs 1, 2, 3, and 4, respectively. As the numerical domain used has size 2π (see above), these values correspond respectively to ion skin depths with associated wave numbers $k_\varepsilon = \infty$, 32, 16, and 8 and to scales of $\rho_{ii} = 0$, 0.03, 0.06, and 0.125.

Figures 1 and 2 show examples of current components. The left-hand panels show, for each run, two-dimensional cuts in the perpendicular plane of one perpendicular component j_x (Fig. 1) and of the parallel component j_z (Fig. 2) for one snapshot of the simulation in the statistically steady state (when $t = 4.5$). The same field is plotted in the right-hand panels with an arbitrary tilt angle in order to highlight the chaotic alternation of positive and negative fluctuations of the fields. From visual inspection, it is evident that structures become more fragmented as ε increases. Figure 3 shows the total energy spectra $E(k)$, integrated on spheres of radius k, for the four runs. The ion skin depth scale is also indicated. Despite the limited wave vector range not allowing the observation of power law scaling, the large-scale part of the spectra is compatible with the typical Kolmogorov scaling $\alpha = 5/3$. For the largest ε (run 4), a secondary scaling region emerges at scales smaller than the ion skin depth, compatible with the typical power law spectrum for reduced Hall MHD, $\alpha = 7/3$.

It was recently stressed that well resolved numerical simulations are necessary in order to accurately quantify high-order statistics and intermittency in MHD [39]. In particular, it has been claimed that if the flow is not properly resolved, a partial thermalization of the small scales may result in artificial Gaussian statistics and an artificial decrease of the intermittency. Wan *et al.* [39] also argued that a MHD simulation can be considered well resolved if the kurtosis of the current is independent of the spatial resolution. In order to evaluate the sensitivity to the grid resolution of our system, two different realizations are performed with higher spatial resolution of $768^2 \times 32$ and $512^2 \times 64$ grid points, respectively. Using the same set of parameters, diagnostics such as structure functions, scaling exponents, and probability distribution functions of field fluctuations are used to show that scaling and intermittency properties are not affected by resolution. In the MHD and HMHD runs analyzed here, the requirement of kurtosis convergence is fulfilled, at least up to the level of expected statistical fluctuations. It is thus possible to conclude that the simulations are well resolved and satisfy the stringent criteria of Wan *et al.* [39]. The resolution analysis is shown in detail in Ref. [38].

IV. SIGNED MEASURE AND CANCELLATION EXPONENT

As discussed in the Introduction, turbulent plasmas are often characterized by the scale-dependent formation of energetic and localized structures. These represent regions where the dissipation of energy is enhanced and are believed to be responsible for the anomalous scaling of the structure functions. Intermittency and multifractality are strictly related to their presence [45]. Structures such as current sheets and vorticity filaments are extensively observed in numerical simulations [30,46–50]. Solar wind measurements have also revealed the presence of structures of different types (current sheets, rotational discontinuities, and vortices) in measured plasmas [51–54]. Since structures can be seen as smooth regions embedded in a highly fluctuating field, their presence and characteristics will influence the statistical properties of

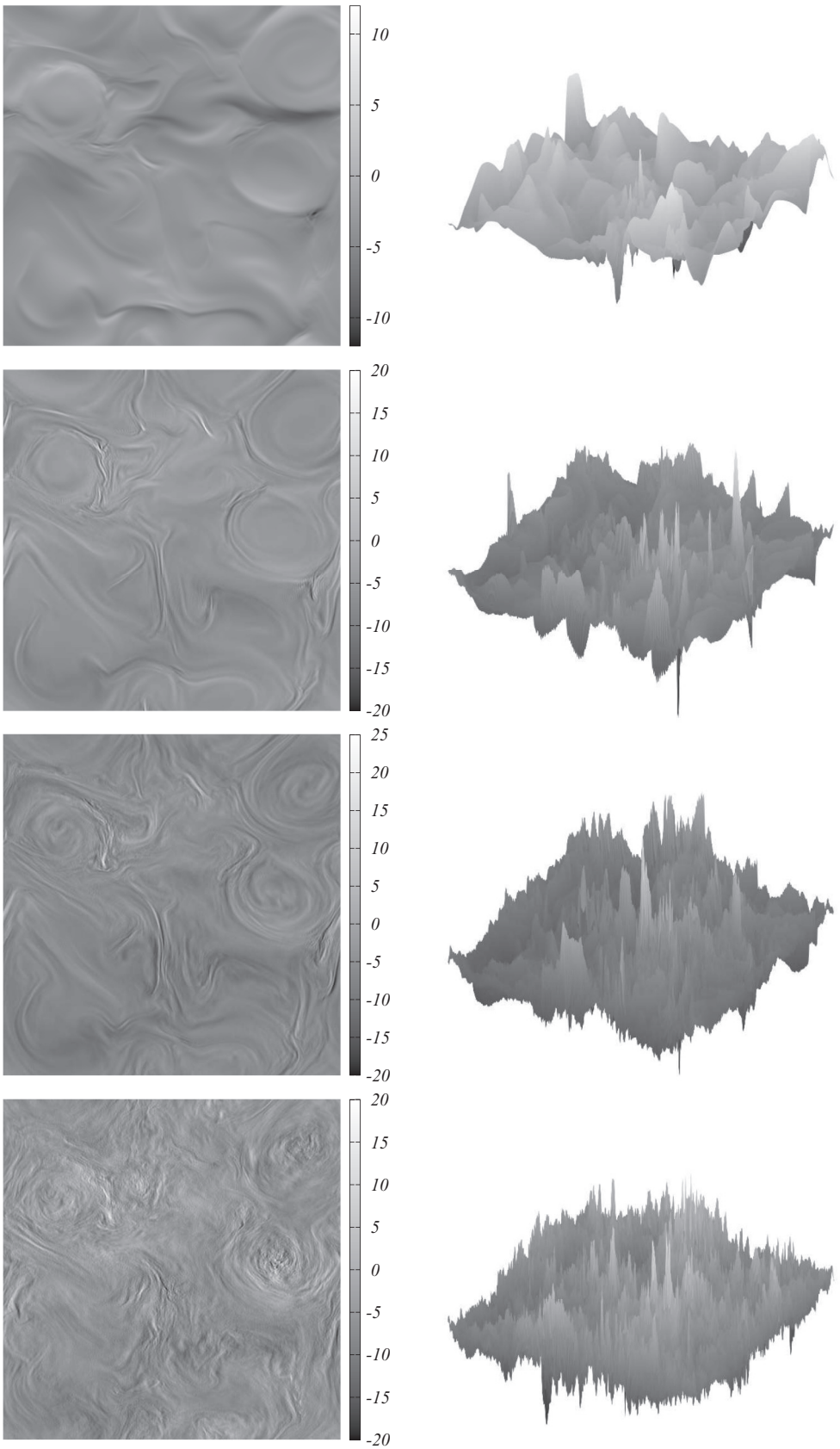

FIG. 1. The left panels show slices of the perpendicular current component j_x (in adimensional units; see Sec. II for the normalization used) in the perpendicular plane for the four different values of ε used in this work (ε increasing from top to bottom). The right panels show the same fields, seen at an arbitrary tilt angle, highlighting the presence of alternate sign structures at all scales. In these panels, the scale of grays is arbitrary.

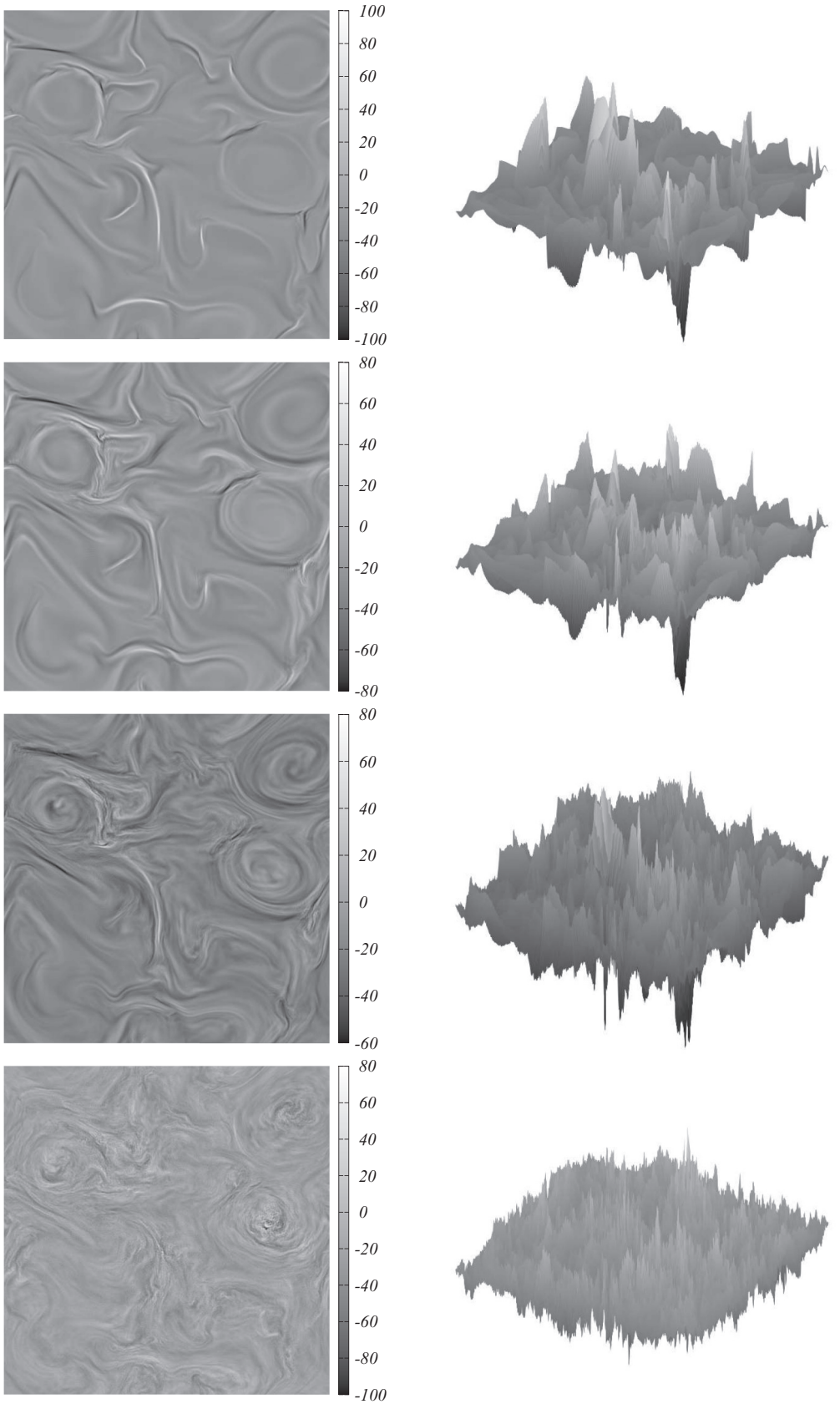

FIG. 2. The left panels show slices of the parallel current component j_z (in adimensional units; see Sec. II for the normalization used) in the perpendicular plane for the four different values of ε used in this work (ε increasing from top to bottom). The right panels show the same fields, seen at an arbitrary tilt angle (arbitrary grayscale).

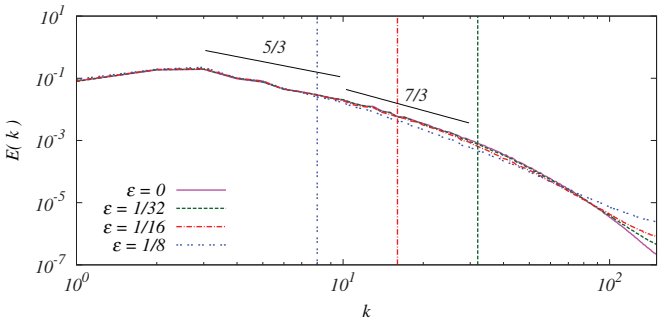

FIG. 3. (Color online) Total energy spectra for the four runs (see the legend). The vertical lines represents the values of the inverse ion skin depth for the three runs with nonvanishing Hall term. Phenomenological predictions for the MHD range and the Hall range are also indicated.

the scale-dependent changes of the sign of the field gradients. It is thus appropriate to investigate the scaling properties of the sign of the field fluctuations. In this paper we make use of a convenient tool based on the concept of sign-singular measure [40], which is described below.

Let $f(\mathbf{r})$ be a scalar field with zero mean, defined on a d-dimensional domain $Q(L)$ of size L. In analogy to probability measures, for each interval $Q(l) \subset Q(L)$ of size l it is possible to introduce a signed measure as the (normalized) mean of the field over the subset

$$\mu(l) = \frac{\int_{Q(l)} d\mathbf{r}\, \mathbf{f}(\mathbf{r})}{\int_{Q(L)} d\mathbf{r} |\mathbf{f}(\mathbf{r})|}. \tag{16}$$

As opposed to positive defined probability measures, the signed measure retains information on the field fluctuation sign. The measure is said to be sign singular if for any size of a subset $Q_A(l)$ for which $\mu_A(l) \neq 0$ there exists a subset $Q_B(l') \subset Q_A(l)$ such that the measure $\mu_B(l')$ has opposite sign to $\mu_A(l)$. This indicates that the measure changes sign on an arbitrarily fine scale [40]. In analogy to the multifractal measure, it is possible to partition the domain in disjoint subsets of size l, $\{Q_i(l) \subset Q(L)\}$, and to compute the measures $\mu_i(l)$ over each subset of the partition. Then the sign singularity of the measure can be quantitatively characterized by introducing the cancellation exponent κ, that is, the scaling exponent of the cancellation function defined as

$$\chi(l) = \sum_{Q_i(l)} |\mu_i(l)| \sim l^{-\kappa}, \tag{17}$$

where the sum is extended to all disjoint subsets $Q_i(l)$.

For a field with both positive and negative structures embedded in a fluctuating field, when the size of the subset $Q_i(l)$ is large cancellations between small structures of opposite sign occur within each box, resulting in a small contribution to the signed measure. However, as the boxes become smaller and reach the typical size of the structures, each box is more likely to contain a single sign-defined structure, reducing the level of cancellations. The cancellation exponent represents thus a quantitative measure of the efficiency of the field cancellations. For example, a smooth field with no sign singularity has a constant cancellation function ($\kappa = 0$), whereas for a stochastic process $\kappa = d/2$ [55]. More generally, if a field $\mathbf{g}(\mathbf{r})$ is homogeneous with a Hölder scaling exponent h, that is, if $\langle \|\Delta\mathbf{g}(\mathbf{l})\| \rangle = \langle \|\mathbf{g}(\mathbf{r}+\mathbf{l}) - \mathbf{g}(\mathbf{r})\| \rangle \sim l^h$, then the cancellation exponent of its derivative $f \equiv dg/dr$ is $\kappa = 1 - h$ [55,56]. Thus the cancellation exponent can be related to the properties of structures. Furthermore, a simple geometrical argument, based on the separation of the field in correlated (the structures) and uncorrelated (the background field) subsets, allows us to establish a phenomenological relationship between the cancellation exponent and the fractal dimension D of the typical dissipative structures of the flow

$$\kappa = (d - D)/2 \tag{18}$$

(see, e.g., [41] for details). It should be kept in mind that, because multifractality is ubiquitous in MHD turbulence, the use of one fractal dimension cannot capture all the features of the scaling. Nonetheless, D still represents a useful indicator for the geometrical characteristics of the mean intermittent structures of the flow. Cancellation analysis has been performed in the past to describe the formation of structures in two-dimensional MHD plasmas [41,57] and successfully applied to solar active regions, where the time evolution of the properties of the photospheric current has allowed the prediction of the occurrence of large flares [58–60]. In this paper we show results of the cancellation analysis of the fields, with the aim of pointing out the effect of the Hall term on the spatial structure of the small-scale fluctuations.

V. RESULTS

For our analysis, we consider four snapshots of RHMHD simulations, performed using four different values of the Hall parameter ε, as indicated in Sec. III. All the snapshots are taken in a statistically steady state of the system, occurring at $t = 4.5$. The fields analyzed here are the three components of the current $\mathbf{j}$ and of the vorticity ω, already shown in Figs. 1 and 2. In order to estimate the cancellation functions, we divided the simulation domain of size $L^3 = (2\pi)^3$ in subsets of variable size $l_x \times l_y \times l_z$ with $l_x = l_y = l_\perp$ and $l_z = l_\parallel$. Note that, in order to maximize the number of possible integer partitions, about 1% of the $L^3 = (2\pi)^3$ domain has been trimmed. This procedure does not affect the results.

Figure 4 shows an example of two-dimensional cuts of the signed measure computed for the parallel component of the current j_z in the plane x-y for $\varepsilon = 1/16$ and for four different partition box sizes. As expected, the coarse graining of the partition leads to cancellations at larger scales, so small-scale structures (the current filaments clearly evident at small scales) gradually disappear. Similar behavior is seen for all fields components and for any value of the Hall parameter larger than zero. In the absence of the Hall effect, structures are smoother and well resolved and the effect of cancellations is less evident.

From the signed measures, the cancellation functions (17) have been computed for all components of the current $\mathbf{j}$ and of the vorticity ω as a function of the two scale parameters $l_\perp$ and $l_\parallel$. Figure 5 shows two examples, for two different components j_x (left panel) and j_z (right panel) at $\varepsilon = 1/16$. The different curves of each panel refer to three different values of the parallel scale $l_\parallel$. While scaling properties are present in the perpendicular direction $l_\perp$, the cancellation function

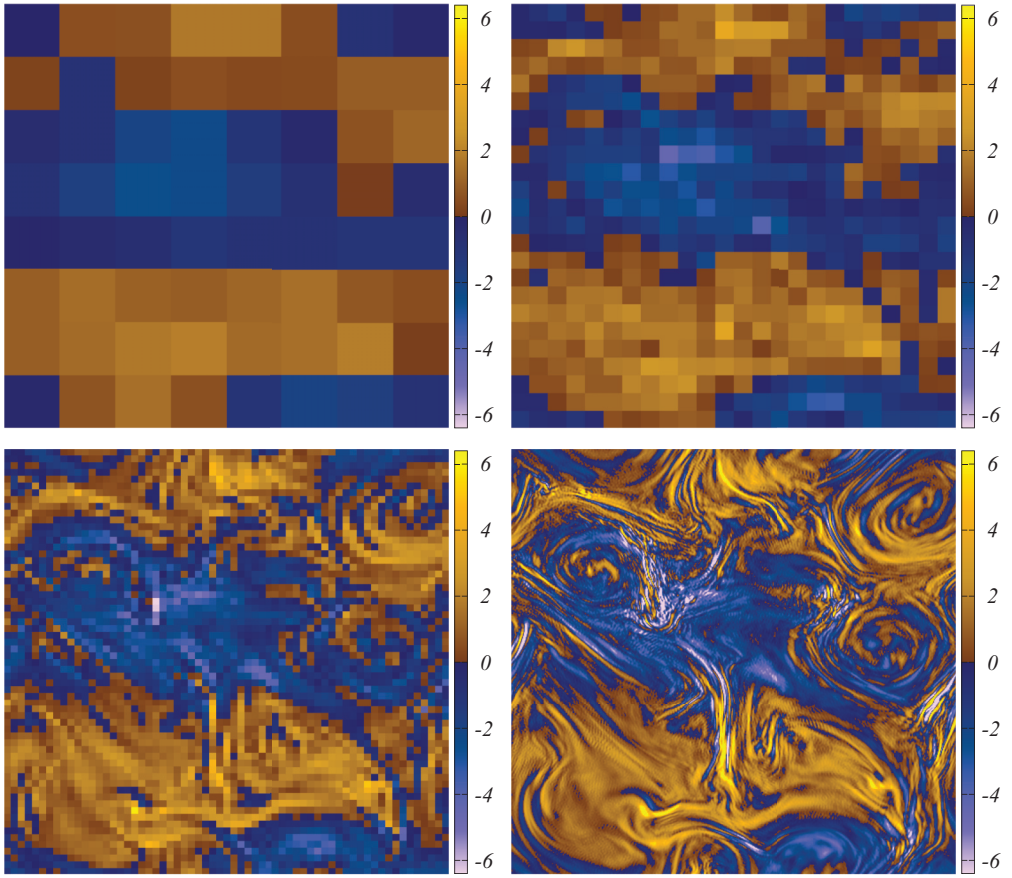

FIG. 4. (Color online) Signed measure μ as estimated for j_x in the y-z plane, shown for run 3 ($\varepsilon = 1/16$), for four different partition box sizes (top left, $l_\perp = 0.12$; top right, $l_\perp = 0.04$; bottom left, $l_\perp = 0.016$; and bottom right, $l_\perp = 0.002$.

decrease with the parallel scale $l_\parallel$ is somewhat smoother and less defined, as will be discussed later. This is due to the fact that in RHMHD the turbulent cascade is mainly developed in the planes perpendicular to the mean magnetic field. For this reason, we will mainly concentrate on the scaling properties in the perpendicular planes, by selecting one particular parallel scale ($l_\parallel = 0.03$), and leave the discussion of the parallel scale decay to Sec. VI. However, we have tested the results for different parallel scales and no significant difference was observed. Figure 6 shows two examples of the variation with ε of the cancellation functions of the current for a fixed value of $l_\parallel = 0.03$. For the perpendicular component of the current j_x (left panel), the change of the scaling properties with the Hall parameter is evident. In contrast, the changes are more subtle for the parallel current j_z. When appropriate, power law fits of the cancellation functions $\chi(l_\perp) = A l_\perp^{-\kappa}$ have been performed through a least-squares method. Two examples of fit are displayed in Fig. 7. For a visual test, the cancellation functions have been compensated by dividing them by the fitted power law $l_\perp^{-\kappa}$, as plotted in the bottom panels of the figure. In this representation, power law scaling ranges are seen as flat regions of the compensated plots. Compensated

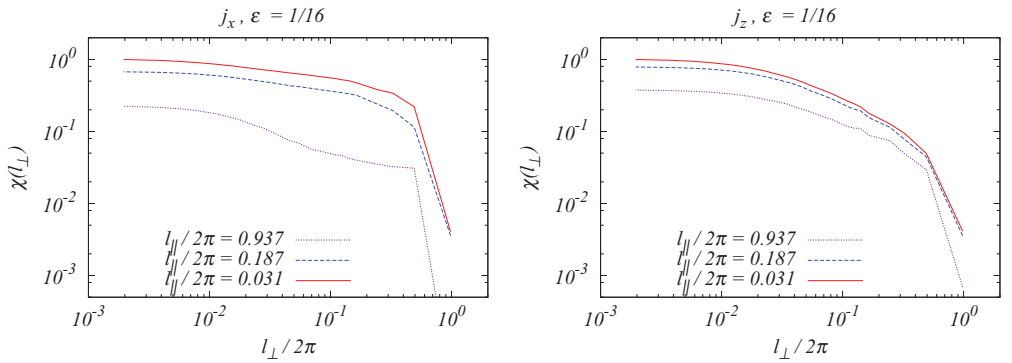

FIG. 5. (Color online) Cancellation function $\chi(l_\perp)$ versus the scale parameter $l_\perp$. The examples given here refer to the current perpendicular component j_x (left panel) and parallel component j_z (right panel) for $\varepsilon = 1/16$.

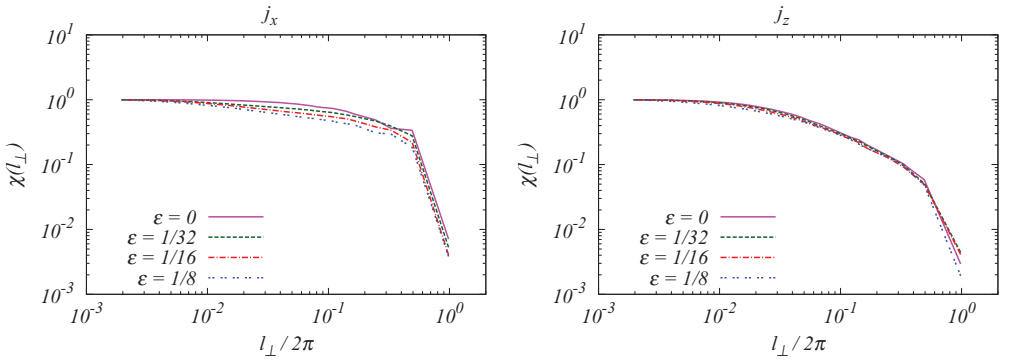

FIG. 6. (Color online) Cancellation function $\chi(l_\perp)$ for the current perpendicular component j_x (left panel) and parallel component j_z (right panel) for four values of the Hall parameter ε (see the legend) at $l_\parallel/2\pi = 0.03$.

plots and fitting power laws are represented by solid lines for the Hall range and double-dashed lines for the MHD range. As can be seen in the examples given in Fig. 7, the cancellation functions suggest the presence of power law scaling, and therefore sign singularity, in a range of perpendicular scales corresponding to the inertial range of the energy spectra (cf. Fig. 3). This holds for all fields and Hall parameters and is the signature of the MHD turbulent cascade among structures of different size [41]. A second power law range emerges at small scales when the strength of the Hall term increases, as in the case shown in the right panel of Fig. 7. This suggests that a secondary sign singularity is present, with fragmentation of dissipative structures along the scales, presumably due to the nonlinear Hall cascade. The small-scale power law is observed for the current and vorticity components lying on the plane perpendicular to B_0, while for the parallel components the secondary sign singularity only appears for the largest value of ε analyzed here. This is in agreement with the emergence of a small-scale power law range in the energy spectra (see Fig. 3), compatible with the HMHD phenomenological spectral index.

As mentioned in the previous section, values of the cancellation exponents provide information on the spatial structure of the fields. In order to discuss more easily the analysis results, the cancellation exponents are converted into the typical fractal dimension of the structures, as $D = 3 - 2\kappa$. Values of D are then displayed in Fig. 8 as a function of ε for the three components of the current [Figs. 8(a) and 8(c)] and of the vorticity [Figs. 8(b) and 8(d)] so that the influence of the increasing Hall effect on the scaling can be evaluated. In the following, we will use the notation $D_\perp^{(f)}$ for the fractal dimension estimated for the perpendicular cancellation function $\chi(l_\perp)$ and $D_\parallel^{(f)}$ for the parallel cancellation function $\chi(l_\parallel)$, where $f = j,\omega$ indicates the field under study. When the superscript (f) is omitted, we are indicating both fields. It is also possible to introduce a parameter for estimating the global fractal dimension of the fields by averaging the three values $D_i^{(f)}$ of the fractal dimension obtained for the ith component of each field f, $D_\perp^{\star(f)} = (D_x^{(f)} + D_y^{(f)} + D_z^{(f)})/3$ (we have temporarily suppressed the subscript $\perp$ in this formula to simplify the notation). We remind the reader that in the RHMHD configuration, most of the nonlinear structures are generated in the plane perpendicular to B_0. Therefore, the parallel components of the current j_z and

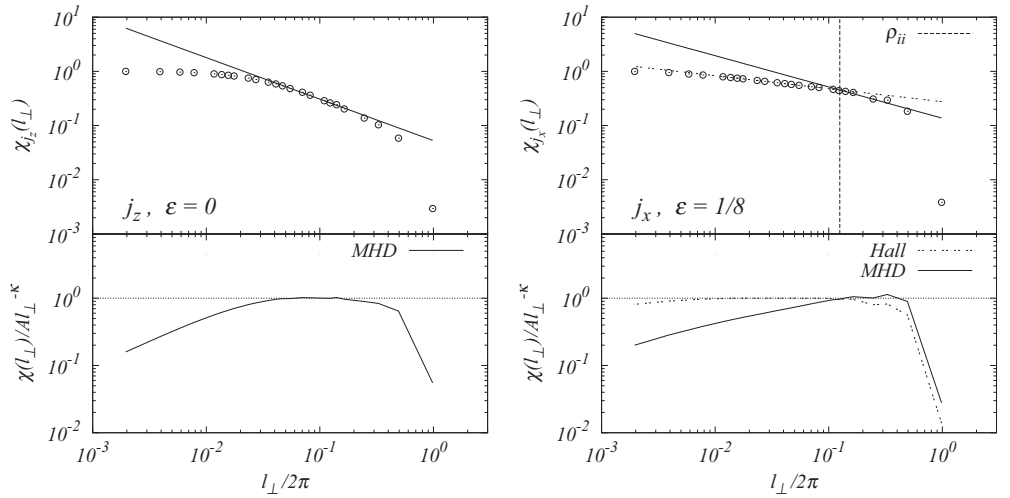

FIG. 7. Examples of fit of the cancellation function, shown here at $\varepsilon = 0$ for j_z (left panel) and at $\varepsilon = 1/8$ for j_x (right panel). The power law fits $\chi(l_\perp) = A(l_\perp/2\pi)^{-\kappa}$ are superimposed (one in the left panel, two in the right panel). The ion skin depth is indicated by the dashed line in the right panel. The bottom part of the right plot shows the compensated cancellation functions $\chi(l_\perp)/A(l_\perp/2\pi)^{-\kappa}$.

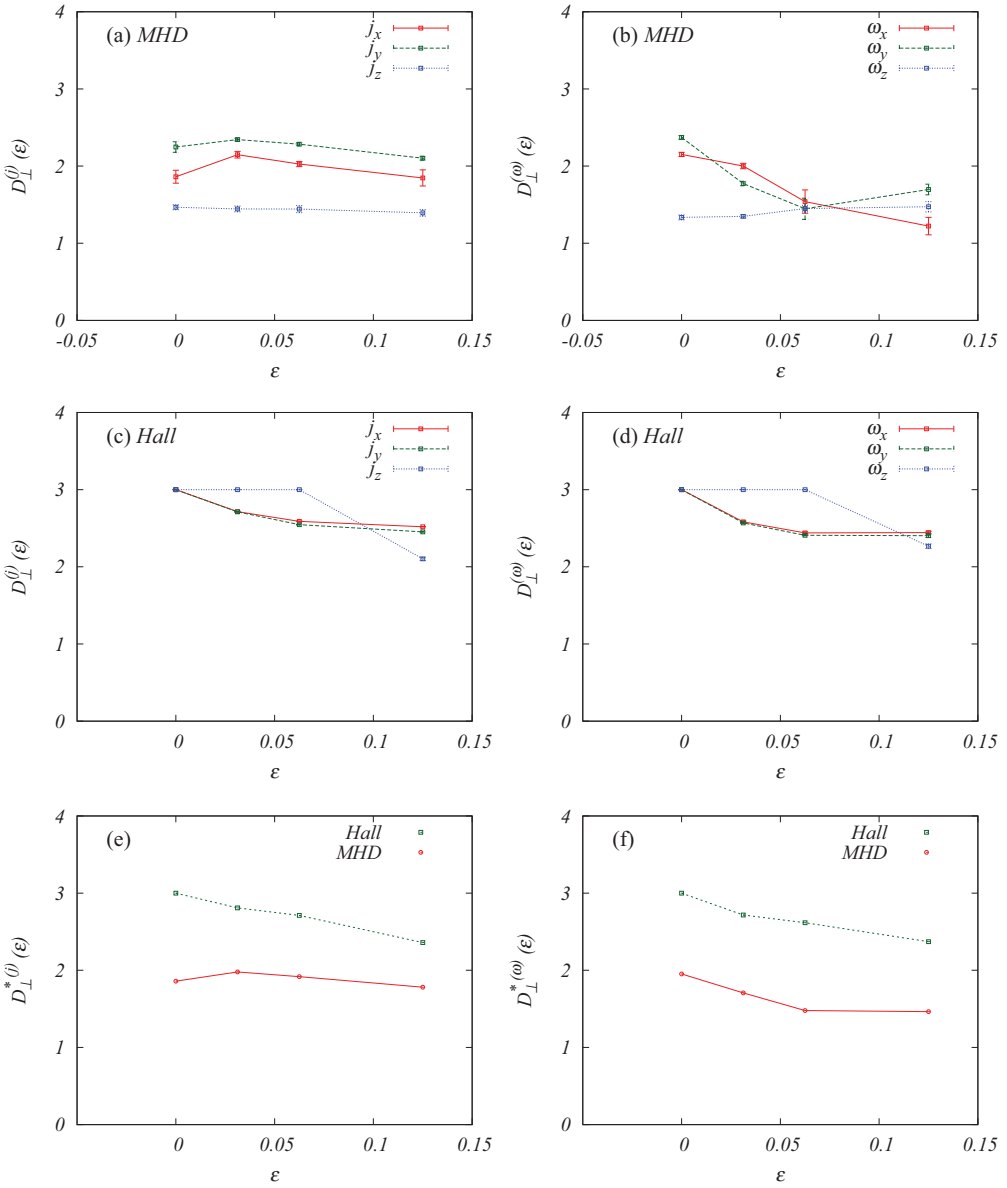

FIG. 8. (Color online) Fractal dimension $D_\perp$ estimated through Eq. (18) for the three components of current [for (a) the MHD range and (c) the Hall range] and vorticity [for (b) the MHD range and (d) the Hall range], labeled with different colors and line style (see the inset). The indicators $D^\star_\perp$ (see the text) are also plotted for (e) and (f) the two fields (black lines).

vorticity ω_z, which depend on the perpendicular components of the magnetic and velocity fields, are of particular interest. The perpendicular components j_x, j_y, ω_x, and ω_y, in contrast, include both the perpendicular and parallel components of the magnetic and velocity fields. This results in mixing the turbulent perpendicular dynamics with the quasilinear parallel dynamics, so the results are not easily interpreted.

In the MHD inertial range, marked "MHD" in the figures, the estimated fractal dimension for the parallel component of the current is almost constant, showing a weak decrease from $D^{(j)}_\perp = 1.5$ in the MHD regime to $D^{(j)}_\perp = 1.4$ in the Hall regime [red plot in Fig. 8(a)]. Similar values, but with the opposite weak trend, are observed for the vorticity ω_z [Fig. 8(b)]. Such values of D are representative of severely disrupted, almost filamented current sheets. The relative independence of $D^{(j)}_\perp$ on the Hall parameter for the parallel components of vorticity and current is consistent with the fact that in the MHD inertial range, the Hall term is not expected to play a relevant role since it should only be effective at smaller scales.

For the current perpendicular components [green and blue plots in Fig. 8(a)], $D^{(j)}_\perp$ starts around 2 (indicating current sheets) with no Hall effect. As the Hall term is turned on, the dimension first weakly increases to about $D^{(j)}_\perp \simeq 2.2$ and then steadily decreases back to $D^{(j)}_\perp \simeq 2$, showing that structures are becoming more complex. This suggests that inertial range fields are reacting to the onset of the Hall effect, probably in response to the inertial range modification. For the vorticity components perpendicular to B_0 [green and blue plots in Fig. 8(b)], the effect of the Hall term is even more evident, causing a decrease of the dimension from $D^{(\omega)}_\perp \simeq 2.3$

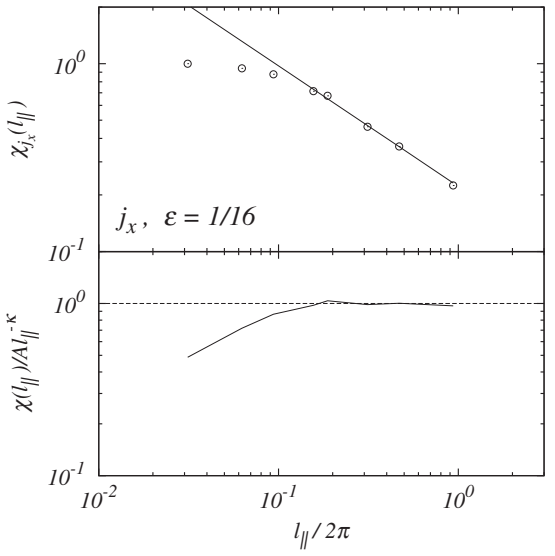

FIG. 9. Cancellation function $\chi(l_\parallel)$ for j_x at $\varepsilon = 1/16$ and for $l_\perp/2\pi = 0.002$. A power law fit is superimposed. The bottom part of the plot shows the compensated cancellation function $\chi(l_\parallel)/A(l_\parallel/2\pi)^{-\kappa}$.

to $D_\perp^{(\omega)} \simeq 1.5$, indicating fragmentation of the vorticity sheets. The global fractal dimensions $D_\perp^\star$ are shown in Figs. 8(e) (for the current) and 8(f) (for the vorticity) for both the MHD and Hall ranges. For the current in the MHD range, the structure's fractal dimension is roughly constant for all values of the Hall effect. Vorticity, in contrast, shows a more evident decrease of the global fractal dimension with ε, from $D_\perp^{\star(\omega)} \simeq 2.3$ to $D_\perp^{\star(\omega)} \simeq 1.5$. This result shows that the magnetic field and velocity are decoupled in the MHD range, so their structures have different fractal properties.

We now turn our attention to the range of scales smaller than the ion skin depth, where the Hall term becomes relevant when ε becomes larger. The results here are very similar for both current and vorticity, suggesting that velocity and magnetic fields decouple only in the MHD range. If no Hall cascade is present ($\varepsilon = 0$), the small-scale range is characterized by smooth fluctuations (for which we assume $D_\perp = 3$) for all components of the fields, as expected when dissipation is active and numerically well resolved. This is reflected in the absence of a power law, or sign singularity, in the transition from the MHD range toward the constant cancellation function value for smooth fields ($\chi = 1 \to \kappa = 0 \to D = 3$) at small scales. As the Hall effect comes into play, the perpendicular components of the current and vorticity start to develop a (poorly defined) power law range, with cancellation exponents κ increasing with ε. The scaling of the cancellation function indicates the presence of strongly persistent structures in the range of scales larger than the typical dissipative scales. In terms of fractal dimension [green and blue plots in Figs. 8(c) and 8(d)], a decrease is observed from $D_\perp = 3$ to $D_\perp \simeq 2.4$, indicating that the smooth fields in the MHD regime (run 1) are developing toward more complex, broken structures (runs

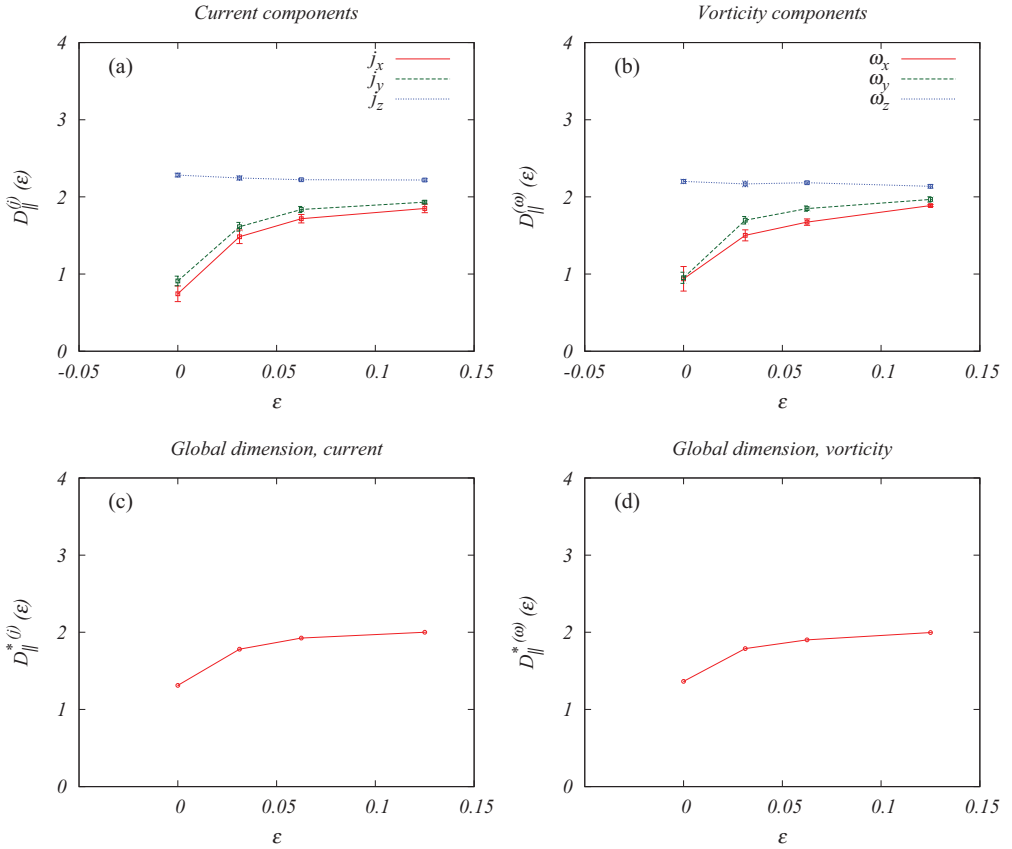

FIG. 10. (Color online) Fractal dimension D of the parallel cancellation function for the three components of (a) and (c) current and (b) and (d) vorticity. The overall indicators $D_\parallel^\star$ are also plotted for (c) and (d) the two fields.

2–4). In contrast, for the parallel component of the current and vorticity the sign singularity in the Hall range is only observed at $\varepsilon = 1/8$. At this value of the Hall parameter, the field is no longer smooth (as for dissipative range), but rather shows the presence of quasi-two-dimensional sign persistent structures [red plots in Figs. 8(c) and 8(d)]. At these small scales, the global fractal dimension calculated for the current and the vorticity steadily decreases from $D_{\perp}^{\star} = 3$ to $D_{\perp}^{\star} \simeq 2.3$ as the Hall term coefficient increases, confirming once more that the turbulent structures are being fragmented by the nonlinear Hall cascade.

Finally, we quickly review the results obtained for the scaling in the parallel direction. Figure 9 shows an example of cancellation functions of the current j_x as a function of the parallel scale $\chi(l_{\parallel})$ and for $l_{\perp}/2\pi = 0.002$. As evident, the power law range is severely reduced because of the lower resolution of the numerical simulations in that direction. However, we have fitted the cancellation functions with the usual power law, obtaining the cancellation exponents κ and therefore the fractal dimensions D. These are shown in Fig. 10 as a function of the Hall parameter. As expected from the RHMHD model, for both fields the component parallel to the magnetic field has almost constant $D_{\parallel} \simeq 2.2$ [see the red plots in Figs. 10(a) and 10(b)]. In contrast, for the two components on the perpendicular plane, $D_{\parallel}$ increases with ε from very small values ($D_{\parallel} \simeq 0.8$) to about $D_{\parallel} \simeq 1.9$ [green and blue plots in Figs. 10(a) and 10(b)], similarly to what is observed for the perpendicular cancellation functions. The global fractal dimension increases from $D_{\parallel}^{\star} = 1.3$ to $D_{\parallel}^{\star} = 2$.

VI. CONCLUSION

In this paper, a set of simulations of a RHMHD flow realized with different values of the Hall parameter ϵ was analyzed by using the sign-singular measure. Scaling of the cancellation function was observed in two distinct ranges of scales, corresponding to the MHD and Hall MHD ranges. This is interpreted as the presence of an active nonlinear turbulent cascade generating structures (i.e., parts of the fields with persistent sign) on all scales. The cancellation exponents, measured by fitting the cancellation functions with power laws, indicate the degree of cancellation occurring between structures of opposite sign and are related to the gross fractal dimension of the typical turbulent structures in the flow. In the MHD range, current structures are only weakly sensitive to the Hall effect, showing slightly decreasing fractal dimension in particular in the perpendicular current components. The vorticity structures have a more evident fragmentation, suggesting that the velocity and magnetic field may have decoupled dynamics in this range. In the Hall range, current and vorticity have similar behavior, showing increasingly unraveled structures. The nonlinear Hall term is thus responsible for disruption and unraveling of the MHD current sheets and for the generation of smaller-scale structures.

The results obtained here, together with previous analysis [29,38], provide a comprehensive approach that helps answer the basic question: Do the current sheets get wider or narrower with the Hall effect? We can conclude that the Hall term has a dual effect on the current sheets at different scales. On the one hand, it increases the macroscale of the sheets by proportionally increasing their characteristic size. On the other hand, it causes these structures to unravel, which corresponds to generating microstructures on smaller scales. The decrease of the fractal dimension is a manifestation of the emerging microscales, while the widening of the macroscale of the sheet produces an increase of the filling factor of these microstructures and the subsequent reduction of the observed intermittency [38].

These results may settle both the numerical and observational debate about the widening vs narrowing of the current sheets, which was probably due the extremely complex nature of the structures. Therefore, a more comprehensive analysis, based on multiple approaches to the same set of data (global magnitudes, characteristic times, energy cascade, intermittency, and geometrical and fractal properties), is desirable in order to fully understand the effect of the Hall term on the flow dynamics and in particular on the fractal characteristics of the current sheets. This work, along with Refs. [29,38], may be an example of such a comprehensive approach.

ACKNOWLEDGMENTS

P.D. acknowledges support from the Carrera del Investigador Científico of CONICET. The authors acknowledge support from ANPCyT Grants No. PICT 2011-1626 and No. 2011-1529, CONICET Grant No. PIP 11220090100825, and Universidad de Buenos Aires Program No. UBACYT 20020110200359. The research leading to these results has received funding from the European Union Seventh Framework Programme FP7/2007-2011 under Grant Agreement No. 269297 “Turboplasmas”.

[1] P. D. Mininni, D. O. Gómez, and S. M. Mahajan, Astrophys. J. **584**, 1120 (2003).
[2] F. S. Mozer, S. D. Bale, and T. D. Phan, Phys. Rev. Lett. **89**, 015002 (2002).
[3] D. Smith, S. Ghosh, P. Dmitruk, and W. H. Matthaeus, Geophys. Res. Lett. **31**, 02805 (2004).
[4] L. F. Morales, S. Dasso, and D. O. Gómez, J. Geophys. Res. **110**, A04204 (2005).
[5] M. Wardle, Mon. Not. R. Astron. Soc. **303**, 239 (1999).
[6] S. A. Balbus and C. Terquem, Astrophys. J. **552**, 235 (2001).
[7] W. H. Matthaeus, P. Dmitruk, D. Smith, S. Ghosh, and S. Ounghton, Geophys. Res. Lett. **30**, 2104 (2003).
[8] P. D. Mininni, D. O. Gómez, and S. M. Mahajan, Astrophys. J. **619**, 1019 (2005).
[9] S. Galtier, J. Plasma Phys. **72**, 721 (2006).
[10] P. Dmitruk and W. H. Matthaeus, Phys. Plasmas **13**, 042307 (2006).

[11] D. O. Gómez, S. M. Mahajan, and P. Dmitruk, Phys. Plasmas **15**, 102303 (2008).
[12] L. N. Martin, P. Dmitruk, and D. O. Gómez, Phys. Plasmas **17**, 112304 (2010).
[13] N. H. Bian and D. Tsiklauri, Phys. Plasmas **16**, 064503 (2009).
[14] G. P. Zank and W. H. Matthaeus, J. Plasma Phys. **48**, 85 (1992).
[15] A. A. van Ballegooijen, Astrophys. J. **311**, 1001 (1986).
[16] D. W. Longcope and R. N. Sudan, Astrophys. J. **437**, 491 (1994).
[17] D. L. Hendrix and G. van Hoven, Astrophys. J. **467**, 887 (1996).
[18] L. Milano, P. Dmitruk, C. H. Mandrini, D. O. Gómez, and P. Demoulin, Astrophys. J. **521**, 889 (1999).
[19] D. O. Gómez and C. Ferro Fontán, Astrophys. J. **394**, 662 (1992).
[20] P. Dmitruk and D. O. Gómez, Astrophys. J. Lett. **527**, L63 (1999).
[21] G. Nigro, F. Malara, V. Carbone, and P. Veltri, Phys. Rev. Lett. **92**, 194501 (2004).
[22] G. Nigro, F. Malara, and P. Veltri, Astrophys. J. **685**, 606 (2008).
[23] P. Dmitruk, D. O. Gómez, and W. H. Matthaeus, Phys. Plasmas **10**, 3584 (2003).
[24] S. Oughton, P. Dmitruk, and W. H. Matthaeus, Phys. Plasmas **11**, 2214 (2004).
[25] P. Dmitruk, W. H. Matthaeus, and S. Oughton, Phys. Plasmas **12**, 112304 (2005).
[26] J. Birn and M. Hesse, J. Geophys. Res. **106**, 3737 (2001).
[27] Y. Ren, M. Yamada, S. Gerhardt, H. Ji, R. Kulsrud, and A. Kuritsyn, Phys. Rev. Lett. **95**, 055003 (2005).
[28] M. Shay, J. F. Drake, B. N. Rogers, and R. E. Denton, J. Geophys. Res. **106**, 3759 (2001).
[29] L. N. Martin, P. Dmitruk, and D. O. Gómez, Phys. Plasmas **19**, 052305 (2012).
[30] S. Donato, S. Servidio, P. Dmitruk, V. Carbone, M. A. Shay, and P. A. Cassak, Phys. Plasmas **19**, 092307 (2012).
[31] P. D. Mininni, D. O. Gómez, and S. M. Mahajan, Astrophys. J. **567**, L81 (2002).
[32] P. D. Mininni, A. Alexakis, and A. Pouquet, J. Plasma Phys. **73**, 377 (2007).
[33] D. O. Gómez, P. D. Mininni, and P. Dmitruk, Phys. Rev. E **82**, 036406 (2010).
[34] M. Yamada, Y. Ren, H. Ji, J. Breslau, S. Gerhardt, R. Kulsrud, and A. Kuritsyn, Phys. Plasmas **13**, 052119 (2006).
[35] O. Alexandrova, V. Carbone, P. Veltri, and L. Sorriso-Valvo, Planet. Space Sci. **55**, 2224 (2007).
[36] O. Alexandrova, V. Carbone, P. Veltri, and L. Sorriso-Valvo, Astrophys. J. **674**, 1153 (2008).
[37] K. H. Kiyani, S. C. Chapman, Y. V. Khotyaintsev, M. W. Dunlop, and F. Sahraoui, Phys. Rev. Lett. **103**, 075006 (2009).
[38] P. Rodriguez Imazio, L. N. Martin, and P. D. Mininni, Phys. Plasma **20**, 052506 (2013).
[39] M. Wan, S. Oughton, S. Servidio, and W. H. Matthaeus, Phys. Plasmas **17**, 082308 (2010).
[40] E. Ott, Y. Du, K. R. Sreenivasan, A. Juneja, and A. K. Suri, Phys. Rev. Lett. **69**, 2654 (1992).
[41] L. Sorriso-Valvo, V. Carbone, A. Noullez, H. Politano, A. Pouquet, and P. Veltri, Phys. Plasmas **9**, 89 (2002).
[42] D. Montgomery, Phys. Scr. **T2**, 83 (1982).
[43] H. R. Strauss, Phys. Fluids **19**, 134 (1976).
[44] S. Ghosh, M. Hossain, and W. H. Matthaeus, Phys. Commun. **74**, 18 (1993).
[45] U. Frisch, *Turbulence: The Legacy of A. N. Kolmogorov* (Cambridge University Press, Cambridge, 1995).
[46] A. Brandenburg, I. Procaccia, and D. Segel, Phys. Plasmas **2**, 1148 (1995).
[47] H. Politano, A. Pouquet, and P. L. Sulem, Phys. Plasmas **2**, 2931 (1995).
[48] R. M. Kerr and A. Brandenburg, Phys. Rev. Lett. **83**, 1155 (1999).
[49] D. Biskamp and H. Welter, Phys. Fluids B **1**, 1964 (1989).
[50] H. Karimabadi *et al*., Phys. Plasmas **20**, 012303 (2013).
[51] P. Veltri, Plasma Phys. Contr. Fusion **41**, A787 (1999).
[52] C. Salem, A. Mangeney, S. D. Bale, and P. Veltri, Astrophys. J. **702**, 537 (2009).
[53] A. Greco, P. Chuychai, W. H. Matthaeus, S. Servidio, and P. Dmitruk, Geophys. Res. Lett. **35**, L19111 (2008).
[54] D. Sundkvist, A. Retinò, A. Vaivads, and S. D. Bale, Phys. Rev. Lett. **99**, 025004 (2007).
[55] S. I. Vainshtein, Y. Du, and K. R. Sreenivasan, Phys. Rev. E **49**, R2521 (1994).
[56] A. L. Bertozzi and A. B. Chhabra, Phys. Rev. E **49**, 4716 (1994).
[57] J. P. Graham, P. D. Mininni, and A. Pouquet, Phys. Rev. E **72**, 045301(R) (2005).
[58] V. B. Yurchyshyn, V. I. Abramenko, and V. Carbone, Astrophys. J. **538**, 968 (2000).
[59] V. I. Abramenko, V. B. Yurchyshyn, and V. Carbone, Sol. Phys. **178**, 35 (1998).
[60] L. Sorriso-Valvo, V. Carbone, P. Veltri, V. I. Abramenko, A. Noullez, H. Politano, A. Pouquet, and V. B. Yurchyshyn, Planet. Space Sci. **52**, 937 (2004).